RESEARCH ARTICLE

Fluctuations in auxin levels depend upon synchronicity of cell divisions in a one-dimensional model of auxin transport

Simon Bellows[1], George Janes[2], Daniele Avitabile[3], John R. King[1], Anthony Bishopp[2], Etienne Farcot [1] *

1 School of Mathematical Sciences, University of Nottingham, Nottingham, United Kingdom, **2** School of Biosciences, University of Nottingham, Nottingham, United Kingdom, **3** Department of Mathematics, Vrije Universiteit Amsterdam, Amsterdam, The Netherlands

* etienne.farcot@nottingham.ac.uk

Abstract

Auxin is a well-studied plant hormone, the spatial distribution of which remains incompletely understood. Here, we investigate the effects of cell growth and divisions on the dynamics of auxin patterning, using a combination of mathematical modelling and experimental observations. In contrast to most prior work, models are not designed or tuned with the aim to produce a specific auxin pattern. Instead, we use well-established techniques from dynamical systems theory to uncover and classify ranges of auxin patterns as exhaustively as possible as parameters are varied. Previous work using these techniques has shown how a multitude of stable auxin patterns may coexist, each attainable from a specific ensemble of initial conditions. When a key parameter spans a range of values, these steady patterns form a geometric curve with successive folds, often nicknamed a snaking diagram. As we introduce growth and cell division into a one-dimensional model of auxin distribution, we observe new behaviour which can be explained in terms of this diagram. Cell growth changes the shape of the snaking diagram, and this corresponds in turn to deformations in the patterns of auxin distribution. As divisions occur this can lead to abrupt creation or annihilation of auxin peaks. We term this phenomenon 'snake-jumping'. Under rhythmic cell divisions, we show how this can lead to stable oscillations of auxin. We also show that this requires a high level of synchronisation between cell divisions. Using 18 hour time-lapse imaging of the auxin reporter DII:Venus in roots of *Arabidopsis thaliana*, we show auxin fluctuates greatly, both in terms of amplitude and periodicity, consistent with the snake-jumping events observed with non-synchronised cell divisions. Periodic signals downstream of the auxin signalling pathway have previously been recorded in plant roots. The present work shows that auxin alone is unlikely to play the role of a pacemaker in this context.

Author summary

Auxin is a crucial plant hormone, which underpins almost every known plant development process. The complexity of its transport and signalling mechanisms, alongside the

inability to image directly, make mathematical modelling an integral part of the research on auxin. One particularly intriguing phenomenon is the experimental observation of oscillations downstream of the auxin pathway, which serve as an initiator for lateral organ formation. Existing literature, with the aid of modelling, has presented both auxin transport and signalling as potential drivers for these oscillations. In this study, we demonstrate how growth and cell divisions may trigger fluctuations of auxin with significant amplitude, which may lead to regular oscillations in situations where cell divisions are highly synchronised. Physiological variations in the timing of cell divisions leads to reduced temporal regularity in auxin oscillations. Time-lapse microscope images confirm this lack of regularity of auxin fluctuations in the root apical meristem. Together our findings indicate that auxin changes are unlikely to be strictly periodic in tissues that do not undergo synchronous cell divisions and that other factors may have a robust ability to convert irregular auxin inputs into the periodic outputs underpinning root development.

Introduction

As a plant hormone playing a key role in virtually every development process, auxin has attracted a huge amount of research since its discovery at the onset of the 20th century [1]. Despite its relatively small and simple chemical structure, auxin affects a wide range of different responses in plant tissues. Conceptually, this indicates that the complexity of its function lies not in its structure, but in the *processes* it participates in. The prominence of a process over its underlying actors is a viewpoint found at least as early as Heraclitus, and which is still significant in contemporary research [2, 3]. The mathematical theory of processes, known as dynamical systems theory, has been significantly developed over the same period as auxin biology [4]. It is able to describe *qualitative* properties of systems evolving in time, in the sense that they remain true for entire ranges of underlying parameterisations. For example, one may aim to predict whether a system has the ability to oscillate spontaneously, for a range of physiologically plausible conditions, rather than look for specific periods or amplitudes occurring with specific parameter values. This is especially relevant to biology, where parameter values are often not known accurately and/or may vary significantly among individuals or species. As some readers may have limited familiarity with this theory, a brief and informal glossary is provided in S1 File.

The processes controlling auxin biosynthesis and catabolism are still a topic of investigation [5]. Auxin triggers cellular responses by means of a either a canonical pathway that results in transcriptional changes and involving protein-protein interactions and feedback [6], or via a quicker non-transcriptional pathway [7]. Despite the large number of genes responding to auxin, we will hereafter use the generic term "auxin response" to collectively designate changes in transcription of these genes. Auxin is moved over long and short distances by means of a complex transport process involving active transport proteins [8].

Although spatial patterns of auxin have been studied using mathematical modelling, this has largely been restricted to static domains. Yet, important auxin responses take place in growing plant tissues, known as meristems. In addition, auxin patterns evolve at time-scales which are comparable to growth. Whilst auxin response can be triggered within minutes [9], oscillations of the DR5 reporter, downstream the auxin response pathway, have been observed to oscillate with a period of 6 to 15 hours [10, 11]. Of comparable periodicity, cell divisions within the root apical meristem vary significantly depending on cell sizes and position, within a range of 10 to 53 hours [12, 13]. The velocity of auxin transport, on the other hand, has been

well studied and experiments give 10mm/h as a typical estimate [14]. Given root meristem sizes of a few dozen μm in Arabidopsis, it is reasonable to expect patterns resulting from polar transport to have settled near equilibrium over division timescales. Consequently, this paper will rely on a quasi-static assumption and focus on how equilibrium patterns of auxin transport are altered by tissue growth.

An important class of models in which growth has been studied are reaction-diffusion models, famously introduced in such contexts by Turing [15]. The effects of growth can be significant [16–25]. However, this is not directly applicable to auxin, as it is actively transported rather than its distribution being controlled purely by diffusion. More precisely, several families of auxin transporter proteins accumulate on sub-domains of cell membranes. The concentration and location of these transporters are dependent on the concentration of auxin itself [8]. This process is not fully understood at the molecular level, and a number of hypotheses and mathematical models have been proposed, often classified into the two families of "flux-based" and "gradient-based" (or "concentration-based") models. In the former, transporters accumulate as a function of auxin flux through membranes, whilst the latter sees auxin difference between neighbouring cells as the driving quantity [26]. Historically, flux-based models were believed to be better suited to linear patterns such as veins, whilst gradient-based models were supposedly more natural candidates for spotted patterns such as phyllotactic arrangements [27, 28]. However, more recent studies show that this classification is inadequate, as both classes of model can indeed generate a wide range of patterns, including both spots and stripes [26, 29–31]. The formation of these patterns differs from reaction-diffusion models. Here, a "flat" steady state becomes unstable and gives rise to patterns as a diffusion coefficient reaches a bifurcation point. In contrast, in a typical flux-based model the homogeneous "flat" steady state is unconditionally stable [32]. In gradient-based models it does not always exist [33].

In addition to steady patterns, there is experimental evidence of more complex auxin motion, such as travelling waves or localized oscillations. For instance, there have been repeated observations of oscillatory signals of auxin responsive genes, in a specific *oscillatory zone* within plant roots [10, 11]. There are also experimental records of complex centrifugal waves of high auxin in shoot apical meristems [34]. Such rhythmic processes are related to the self-similar structure of plants, where near-identical organs repeatedly emerge from growing meristems [35]. Using mathematical analysis, oscillations have been shown to occur in both classes of transport models via a so-called Hopf bifurcation [32, 33]. However, the shape of these differs drastically from experimental observation. Travelling waves have also been analysed in [36]. In [37] all three processes of signalling, flux transport and growth appear, but no cell division and an hypothetical link between signalling and transport. The work shows how oscillations may occur at a single cell level. A long-standing strategy in modelling auxin transport has been to use computer simulations with parameters tuned to produce plausible patterns [38–43], including a signalling module on a growing root template which shows consistency with experimental data [44]. However, that work uses a pre-defined periodic input, rather than showing emergent oscillations. Another group used computer simulations on a realistic root template to show how patterns of cell divisions are sufficient to induce auxin oscillations, via a mechanism they term reflux-and-growth [45, 46]. Experimental data to date indicates an oscillation in auxin response.

Here we uncover and classify families of auxin patterns in tissues that grow and cells that divide, using dynamical systems theory. We rely on a well established auxin transport model where this systematic approach has already been performed in a static context [33]. It is known that auxin transport models can lead to a large number of co-existing patterns. Each pattern corresponds to a different distribution of auxin within a tissue and is attained from a specific ensemble of initial auxin distributions. Tracking these patterns as a parameter is varied

leads to a curve, with folds occurring for each possible pattern, hence the use of the term 'snaking diagram' in the literature to refer to these folds. Our Results include a review of this snaking phenomenon with a static one-dimensional template. We show how growth and cell divisions induce new behaviour including sudden changes in auxin maxima, which we term snake-jumping as they are explained by overlaying snaking diagrams occurring for different configurations of cells. When cell divisions occur synchronously this can lead to localized oscillations of auxin. By adding some randomness to cell sizes and division events, a loss in the regular periodicity of auxin leads instead to more unpredictable fluctuations. We then present 18 hour time courses of the DII:Venus auxin reporter [47], which are consistent with our numerical results with asynchronised cell divisions.

Results

Simulations on a static domain

Before describing the effects of auxin distribution in a growing tissue, we first present the case of a static domain. These simulations will provide a framework for the later sections where we focus on the effects of growth.

The model we use was first published in [38]; it includes auxin concentration, and the concentration and subcellular localization of the PIN transporters on a linear template. The flux of auxin between cells is mediated by both diffusion and active transport. PIN activity is dependent on auxin levels and gradients between cells, similarly to other concentration based models [28, 29, 38, 39]. See Materials and methods with experimental data for equations and overview figure. Our template comprises around 128 cells (depending on simulations) arranged in single file. One end of the domain allows no flux and represents the root apex, whilst the other end is open ended representing a boundary with the mature root. Essentially this could represent a single file of cells within a root. We have selected this simple template as it allows for more exhaustive analysis including systematically examining the existence of multiple steady states and incorporation of growth dynamics. Our template is much simpler than those used in the previous studies [28, 29, 38, 39], however it has the advantage that we can more easily modulate cell division. Our research takes a subtly different approach to many previous studies. Instead of attempting to recapitulate experimental observations *in-silico*, we use the model to explore what patterns are possible, and only then look if these can be observed *in-planta*. Note that the key property discussed below, i.e. the existence of a snaking bifurcation diagram, is not specific to this template and persists for instance in two-dimensional domains [33].

We ran simulations using parameter sets listed in Table 1 but with variations in the auxin transport (parameter T). To find all steady states as T varies, we employed the numerical continuation algorithms from [48], which we implemented in Matlab in [49]. For low values of T (below 1.9), we see a single steady state solution with high auxin throughout the tissue, which we hereafter term a proto-peak (Fig 1**B**). With increasing of T (2.1), multiple steady states exist for the same value. In a template of 128 cells, this identified multiple steady states with the numbers of peaks varying from one to nine. These patterns co-exist for a given value of T (Fig 1B and S1 Video). The addition of a peak corresponds to a separate bifurcation event materializing as a fold in the bifurcation diagram (Fig 1A), with multiple folds termed as snaking. These results are similar to previous observations [33], providing confidence to move to dynamic templates.

The steady state solutions can be divided into stable states that are robust to small perturbations in auxin distribution, and unstable states which revert to a stable state upon minor changes in auxin. Although we show unstable solutions in S1 Fig, these represent theoretical scenarios: as in any physiological system, even the slightest perturbation (e.g. a 10^{-18}% change

Table 1. Table of default parameter values. Parameter values are partly arbitrary, chosen both to match previous literature and to avoid physical implausibility. Spatial units are expressed in terms of a typical length scale $\mathcal{L}$, indicative of an average cell dimension, of the order of 10–$100\mu m$. Note that the exact value of $\mathcal{L}$ does not affect the relative magnitudes of spatially dependent parameters, as seen from their occurrence in the model equations and in this table. In the model without growth, cell volumes are set to 1 (i.e. $\mathcal{L}$).

Variable	Value	Description
ρ_{IAA}	0.85 ($nmol \cdot \mathcal{L}^{-3} \cdot min^{-1}$)	Auxin production rate
κ_{IAA}	1 ($nmol^{-1} \cdot \mathcal{L}^{3}$)	Michaelis constant for auxin synthesis
μ_{IAA}	0.1 (min^{-1})	Auxin decay rate
D	1 ($\mathcal{L} \cdot min^{-1}$)	Auxin permeability
T	Specified with simulations ($\mathcal{L} \cdot min^{-1}$)	Active transport coefficient
c_1	1.099 ($nmol^{-1} \cdot \mathcal{L}^{3}$)	Exponentiation base for PIN relocation
κ_T	1 (dimensionless)	Auxin transport saturation
ρ_{PIN0}	0 ($nmol \cdot \mathcal{L}^{-3} \cdot min^{-1}$)	Base production of PIN
ρ_{PIN}	1 (min^{-1})	Auxin dependent rate of PIN production
κ_{PIN}	1 ($nmol^{-1} \cdot \mathcal{L}^{3}$)	Michaelis constant for PIN production
μ_{PIN}	0.1 (min^{-1})	PIN decay rate
g	$1/3000$ ($\mathcal{L}^{3} \cdot min^{-1}$)	Growth rate of a cell
V_{max}	$4/3$ ($\mathcal{L}^{3}$)	Volume at which cells divide or stop growing
A_{ij}	1 ($\mathcal{L}^{2}$)	Surface area inter cells i and j

https://doi.org/10.1371/journal.pcbi.1011646.t001

in auxin concentration) would revert to a stable steady state such as those in Fig 1. These unstable branches are however pertinent to understand the dynamics of the system. They may furthermore gain stability as the domain geometry changes through growth, the topic of next section.

Overall, the number of branches in the snaking region is limited by the length of the domain. In line with this, if the domain were unbounded there would be an infinite number of branches. It should be noted that these branches are themselves shadowed by branches containing solutions of permutations of unstable peaks, as shown in S1 Fig. This is likely caused by this
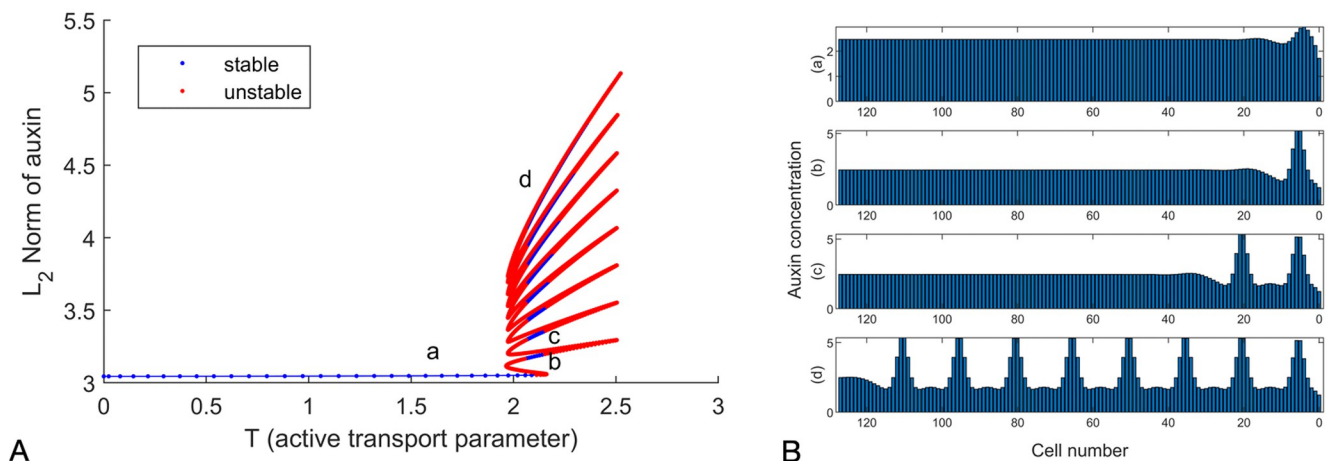
Fig 1. Active transport can lead to multiple stable patterns in auxin concentration. A: The L_2 norm of auxin in the tissue (representative of its total amount) is used in ordinate with active transport parameter T on the x-axis. This is sufficient to distinguish multiple solutions (a)-(d), as well as others found as the transport coefficient T is used as bifurcation parameter. Shown here is the end result of the analysis, see S1 Video for an animated view of the construction of this snaking diagram. B: Example stable solutions marked in A, including the "proto-peak" (a) and 1, 2 and full peaks in a row of 128 cells (corresponding to branches b,c and d on 1A.) for Eqs (1)–(4) with $T = 2.1$ and other parameters as shown in Table 1.

https://doi.org/10.1371/journal.pcbi.1011646.g001

taking place on a finite domain, and in [50] this is shown for the well known Swift-Hohenberg reaction diffusion model, specifically when the peaks get within half a wavelength of the boundary. As such, in the present case, this systematically occurs due to the location of the first peak.

The main observation at this point is that a variety of 'peaked' patterns coexist along a snaking diagram. This general property is robust to an extent but this depends on the underlying tissue geometry. All cells are the same size within the template used. This is a simplification of root anatomy where has been shown that cells further away from the root meristem can be significantly (10 times) larger than those at the tip [51]. Therefore, we also considered a tissue with cell sizes varying in this wider range, see S2A and S2B Fig. Simulations in this template revealed that higher values of the transport parameter T are required to create multiple peaks of auxin, and it was more typical to have a single maximum near the tip. This lower level of multistability is consistent with experimental observations, which do not typically report high numbers of auxin response maxima [8, 10, 11]. Within both templates, it remains true that auxin patterns vary if the tissue geometry is altered, as confirmed in S2C Fig where an auxin maximum can be removed by changing the cell volume.

Simulations with deterministic growth

We next tested the effect of growth and cell division upon the snaking diagram. We report results on numerical simulations of the model (5)–(7) on a growing linear chain, using the procedure described in Materials and methods with experimental data. Starting with a pair of cells, we considered a chain in which only the rightmost eight cells could divide. This is a simplification of the Arabidopsis root, in which typically the 30 or so most proximal cells divide.
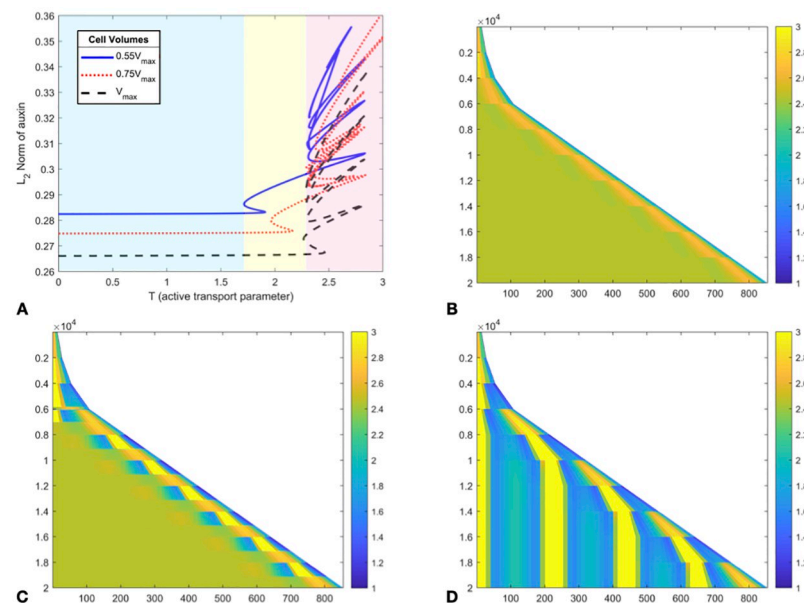
Fig 2. Regular cell divisions produce oscillatory patterns of local auxin accumulation. Growth only occurs for the 8 rightmost cells with the model (5)–(7). A: Continuation in T, for three different cell volumes overlaid. Shaded regions correspond to cases 1–3 discussed in the main text. B-D Time-stepping of the same model, with time as y coordinate, increasing downwards, for different values of T. The x-axis represents cell volumes, scaled so $V_{max} = 10$ (to be indicative of typical cell volumes in pL). B ($T = 1.5$, case 1): the proto-peak is maintained despite growth. C ($T = 2.0$, case 2): the system alternates between two distinct one-peak solutions. D ($T = 2.5$, case 3): new peaks appear over time near the right end of the domain. See also S2 Video for animated versions of B-D.

The 8 end cells elongate at constant rate until they reach a specified maximum volume V_{max}, at which point a cell splits into two daughter cells of volume $\frac{V_{max}}{2}$. This simple cell division model is supported by some experimental evidence [13] but remains a necessary simplification of the more complex growth rate seen in real roots, which varies depending on the cell's position [51]. See Materials and methods for complete details. We used the same ODE parameters as previously and reported in Table 1, where only the transport rate T is left unspecified since we use it as the main bifurcation parameter.

Note that, for the purpose of visual representation in subsequent figures, cells are depicted as rectangles with an arbitrary width and a length proportional to the volumes V_i used in the model equations. This does not entail any loss of generality since the model does not depend on a specific cell geometry but on cell volumes and cell-to-cell contacts, and only linear chains of cells are considered. Also, as discussed under Table 1, units of length can be scaled without effect on the model. Hence the use of any multiple of V_i on the x axes of figures is a valid representation of the model geometry.

However, the relative sizes of cells within a domain are expected to have an effect on patterning. Indeed, in the literature on snaking diagrams it has been shown that the precise arrangement and number of folds depends on the domain geometry [52]. By including growth of the template within our model, one can therefore expect dynamical changes in auxin pattern amongst a wide range of evolving templates.

As cells change in length from their minimal size just after a division event to their maximal size, the snaking diagram shifts and changes in shape (Fig 2A). When cells at the right end of the template (representing meristematic cells) are smaller, then the occurrence of a steady state of auxin with one auxin peak is restricted to lower values of T. Conversely, as cells elongate, the occurrence of the same peak is restricted to higher values of T. This confirms that cell size has a profound effect on determining the available auxin maxima within a tissue.

We observed three qualitatively distinct behaviours, as shaded on Fig 2A. These three regimes are reached for increasing values of T in the order below:

Case 1 (*Low T*) The system stays locked to a proto-peak similar to the static case shown in Fig 1A (a), see Fig 2B.

Case 2 (*Intermediate T*) The system switches from the proto-peak state to a single peak of auxin, see Fig 2C. The transition from a proto-peak to a single peak can occur at lower levels of T than in the static model, due to changes in cell sizes.

Case 3 (*High T*) The system stays locked at a state of maximal peaks with the even expansion of the template causing the creation of regularly spaced new peaks over time, see Fig 2D.

Our categorisation can be systematised by considering bifurcation diagrams. For example, one can see in Fig 2A, that the snaking bifurcation diagram is altered as cell sizes are assigned different values. Therefore, the alteration may correspond to a change in the number of steady states, or simply in their location in state space. At a cell division event, cell sizes are suddenly halved, so that the steady states available in the system correspond to different snaking diagrams out of Fig 2A. Thus, even if the system may not evolve fast enough to be close to a new steady state, the fact that steady states are altered entails a re-direction on the transient dynamics, resulting in noticeable qualitative change. As this is well captured by superimposing snaking diagrams shown in Fig 2A, we casually refer to this general phenomenon as *snake jumping* in the following, as any prior occurrence of the term is from an unambiguously different context [53].

Over time, the cell size V varies in the range $[V_{max}/2, V_{max}]$. Therefore, it follows that the bifurcation diagrams (in T) obtained for fixed volumes of $V_{max}/2$ and V_{max} respectively, will

bound the set of all snaking diagrams obtained for other values of V. As both the $V_{max}/2$ and V_{max} diagrams have a similar shape to that observed in the static simulations in Fig 1A, it is expected that a single branch will be available regardless of V for lower values of T. For intermediate values of T, this will likely correspond to a coexistence of steady states allowing snake jumping to occur.

The diagrams in Fig 2A illustrate how the first snaking curve occurs for different T as cell volume varies. The case 2 patterns are caused by the state jumping between one and no peaks, as seen in Fig 2C. This is further confirmed by taking V as a parameter and continuing solutions: one can see the occurrence of a bifurcation enabling a snake jump from a single full peak to a proto-peak, see S2 Fig. Note that for larger values of T, the system becomes locked to the fully patterned state, where peaks are spread over the whole domain.

One observation that can be made is that the auxin concentration oscillates near the tip of the domain for intermediate values of T. This appears in Fig 2C, and is made more apparent using a video animation of the time-stepping, see S2 Video. Oscillations of auxin response in time have been observed in the model plant *Arabidopsis thaliana* [10, 11] as discussed further in the final section.

Effect of irregularity in cell divisions

A limitation of the simulations discussed in the previous section is that within the dividing zone $\mathcal{D}(t)$ all cells divide simultaneously, since they are initialised at the same size, grow at the same rate and divide at the same threshold. This is not only unrealistic, but it may invalidate our reasoning about snake jumping inducing auxin oscillations. Indeed, the well separated bifurcation diagrams in Fig 2A correspond to domains where a significant number of cells have a different size. In contrast, one may expect less distinctly separated bifurcation diagrams for uneven distributions of cell sizes with less drastic differences (for instance when cell divisions are asynchronous), obstructing snake jumps.

Thus, given the key role played by cell division, and the fact that the timing of cell divisions and the resulting cell sizes are variable within a growing tissue, we carried out simulations where the size of the daughter cells after a division event included some randomness, see Materials and methods for details. In previous analyses we had a scenario in which cells grew linearly and divided when they reach a size V_{max}, at which point they were split into two cells of half that size. Now, the same linear growth and threshold apply, but daughter cells have uneven sizes, chosen randomly. As a result, the distribution of cell sizes and hence the timing division events lose the complete determinism and homogeneity seen in previous simulations.

Hence, the main finding resulting from this study is that if the variability in cell division is kept low, the occurrence of regular oscillations was unlikely. The correlation between cell size at the onset of division has been studied in the shoot apical meristem, where it has been shown to be highly variable [54]. In the root meristem, recent studies using live imaging of growing root meristems show that cell divisions do not occur at once, but over a wave of around 10 hours [55]. The rate of cell divisions are also variable dependent on cell type and position within the meristem [12, 56]. Though presenting some regularity, all available data on roots indicate a significant variability in the timing of cell division events among neighbouring cells. This is illustrated in our study within Fig 3, where we compare simulation results for two values of the standard deviation of cell ratios after a division event. The low value ($\sigma \approx 2.3$) was the highest value we found to ensure qualitative agreement with the perfect synchrony studied above. This is in contrast with the higher variability ($\sigma \approx 9.3$), which is based on the only experimental estimates we have found for σ in the literature [54]. As seen by comparing Figs 2C and 3A (obtained for very similar values of T), the low σ simulations are in good (but not
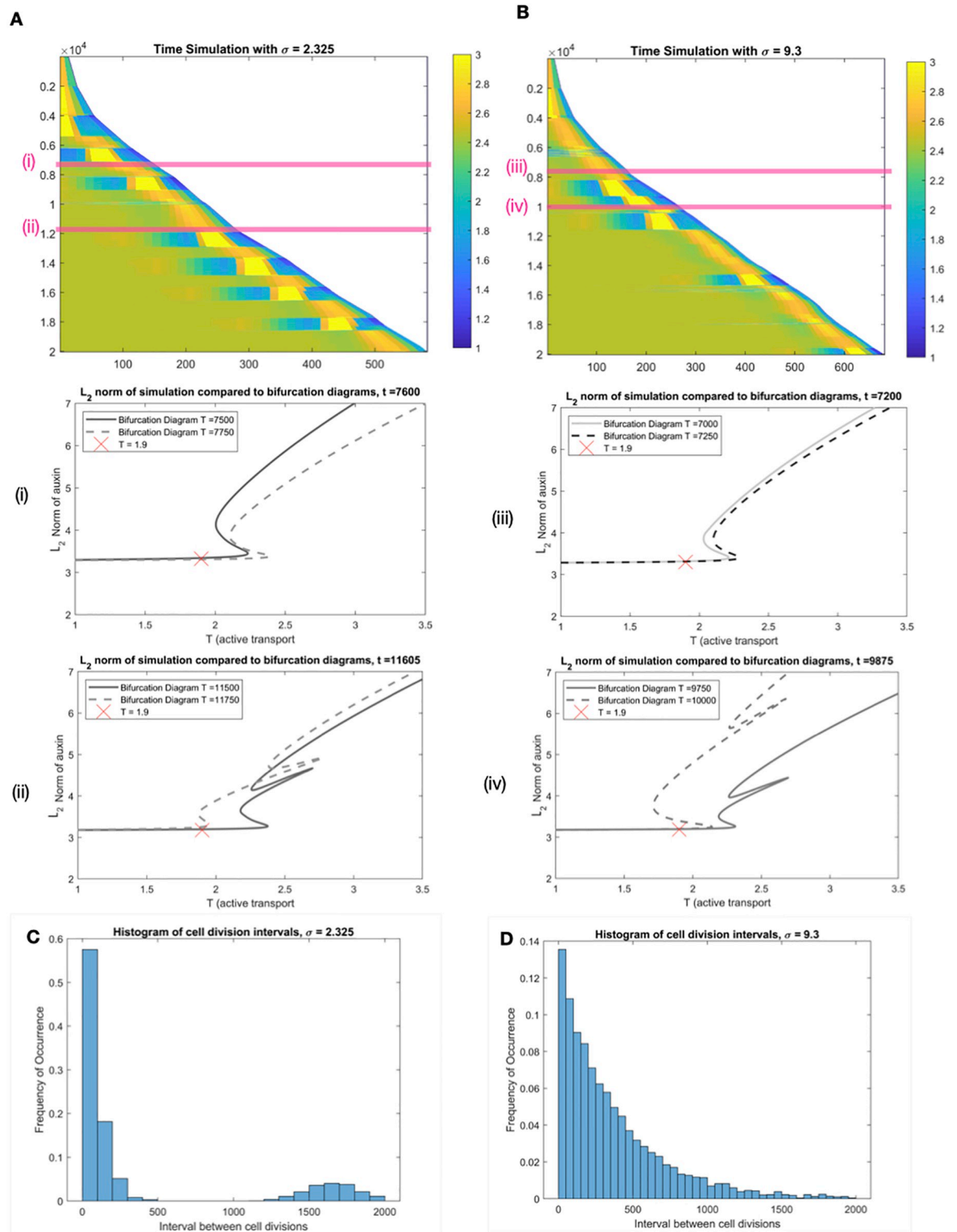
Fig 3. Asynchronous cell divisions trigger irregular auxin fluctuations. Time courses on a growing domain with $T = 1.9$, time in y and space in x coordinates, respectively. Cell sizes after division events are random, with standard deviations $\sigma = 2.325$ (A) and $\sigma = 9.3$ (B). The latter is comparable to experimental data. Histograms (C-D) indicate the distribution of time intervals between division events; a local maximum occurs in C, representative of an emerging periodicity, whereas D has no apparent period. In both cases, transient peaks of auxin coincide with snake jumping events; this is highlighted at two time intervals for each σ (pink bands in A and B): no snake jumping occurs over time intervals (i) and (ii), some do over (iii) and (iv). Over the full course of the simulations, the snaking diagrams gets continually distorted by changes in tissue geometry; see S4 and S5 Videos for animations, of which panels (i)-(iv) above are snapshots, and S3 Video for a deterministic analogue.

complete) agreement with the perfectly synchronised cell divisions. On the other hand, the more realistic dispersion, Fig 3B, leads to a significant irregularity in the changes of auxin peak distribution. This includes short lived travelling waves of auxin, which may appear transiently as an oscillation but have no clearly definable periodicity over the long term (see time 0.6e4 in Fig 3B). As an estimate of periodicity, we computed the distribution of time intervals between successive division events (Fig 3C and 3D); a positive value, corresponding to emerging periodicity, could be detected for low σ only.

Importantly, the underlying mechanism of snake jumping occurs regardless of σ: when a tissue is fixed, for a range of values of the transport parameter T there is a snaking diagram, with coexistence of multiple peaked patterns. Any change in the tissue geometry will induce a deformation of this diagram. Hence as the tissue grows and cells divide, the branches available for a snake jumps vary in a less stereotypical and predictable way than for synchronous cell division, where the overall tissue geometry is much more constrained.

Comparison with experimental data

To explore whether these findings tie with experimental evidence requires temporal data on auxin distribution in a growing root tissue. We generated experimental data reporting auxin levels in roots. Our model predicts that in a growing template with asynchronous cell divisions (as would occur naturally), we should not expect to see a regular oscillation of auxin.

As mentioned in the introduction, there is solid experimental evidence of an oscillatory zone in plant roots. However these data do not include auxin itself but the DR5 reporter [57], which accounts for the transcriptional response to auxin. This response occurs downstream a signalling pathway involving a complex series of nonlinear processes and feedback loops, and has been previously described using differential equation models, see e.g. [58, 59]. Both this modelling work and experimental data indicate that the outputs of the pathway may differ significantly from its auxin input.

Since all results presented above concern the distribution of auxin, without any representation of the signalling pathway, it was difficult to make a direct comparison with DR5 data. The DII:Venus [47] fluorescent reporter is directly degraded by auxin. As such it is more directly representative of auxin concentration than DR5, and therefore a better candidate to support or discount the claims of the previous sections. On the other hand, while data in e.g. [11, 44] relied on the DR5:LUC construct, which allows live time-lapse imaging over long periods, DII:Venus requires a confocal microscope. This provides higher spatial resolution in which auxin (using DII as a proxy) can be quantified in individual cells. We imaged DII expression in 9 *Arabidopsis* roots at 1h time intervals for 18h, and quantified the fluorescence, see Materials and methods with experimental data. These experimental time series are reported on Fig 4.

We did not observe a clear periodic signal in any of the roots that were tracked. We note that almost every root there undergoes noticeable fluctuations over time and space. The temporal profiles show sharp periods of increase and decrease of the fluorescent signal, which can be localized within the tissue. These fluctuations are reminiscent of the simulations performed in the previous section and therefore we attempted a more careful comparison. It is important to note that the experimental set up required to image these roots required a brief reorientation of roots (see Methods). Since auxin is known to be responsive to changes of the gravity vector [60], it is possible that this reorientation may have masked some oscillations.

In Fig 5, we report some selected simulations as well as DII:Venus time series. Note that, due to DII:Venus being an inverse reporter degraded by auxin, the time series were 'reversed' (i.e. taking the difference between the maximum value over time and the full time course, for
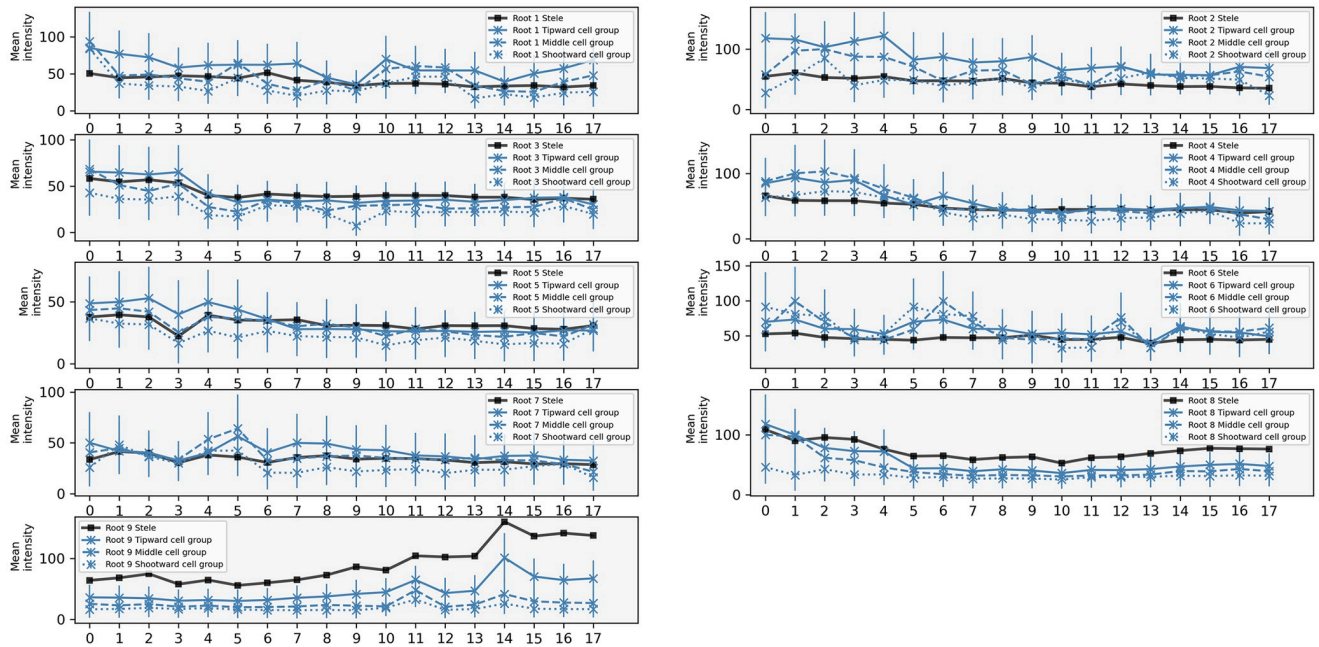
Fig 4. Time series of DII:Venus data. On each graph the three blue cross curves represent three successive groups of five cortex cells from the root tip, while the black curve with squares is a sample of cells from the stele. Curves represent the average intensity over the corresponding cell groups (with three replicates, see text), and error bars the corresponding standard deviation. See protocol in Materials and methods for further details and full data set in S3 File.

https://doi.org/10.1371/journal.pcbi.1011646.g004

each time course). This matching was obtained by trial and error, relying on the randomness in the simulations: a long time-stepping simulation was compared by eye to the DII:Venus data. Although a more robust statistical comparison would have been preferable, the comparable time scales between auxin fluctuations and the longest feasible experimental set-up forced us to resort to this more qualitative approach.

Discussion

All the results presented above aim to clarify behaviour of an established auxin transport model on growing domains. A key technique in this endeavour was numerical continuation (see S1 File for background and S2 File for our implementation), whereby a user systematically scans a full range of possible auxin patterns rather than running individual simulations. The active transport coefficient T is used as bifurcation parameter on "snapshots" of the domain at specific time points during growth. This shows a specific set of stable steady states (auxin patterns) for each time point, forming a snake-like curve as T varies. Each fold of the snaking structure corresponds to a pattern and all patterns compete, attracting distinct sets of initial conditions. Over time, changes in this snaking curve induce changes in which particular pattern attracts the dynamics, leading to potential alternations of patterns across time. We chose to term these alternations snake jumps in reference to the underlying bifurcation diagrams.

In cases where cell divisions are highly synchronised, the number of tissue configurations is strongly limited: all possible tissues are essentially related to each other by a scalar factor (the size of growing cells), ranging over a compact interval. In this scenario, the two extreme values for this factor (just before and after division) provide only two snaking diagrams. Yet, the high number of branches and their associated auxin patterns lead to a range of possible behaviours.
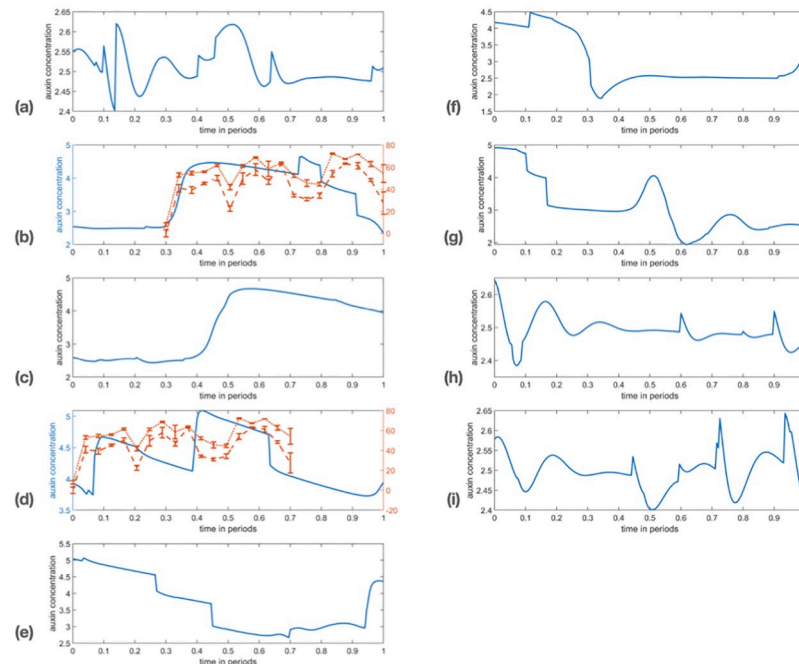
Fig 5. Simulations in qualitative agreement with DII:Venus data. Horizontally: time, normalised to a 'period' of 200 time units. Vertically: mean auxin concentration for cells 6 to 10 over the reference time period. See full time series data and further details in S3 Fig. The parameters for the simulation are as in Table 1, with the exception of cell growth rate being increased by a factor of 10 to allow for longer time range, cell size variability $\sigma = 9.3$ and $T = 1.9$. To highlight agreement, periods in (b) and (d) panels are overlayed with the two tipwards cell groups from root 1 (dashed and dotted from first panel in Fig 4); since DII is a negative reporter, the latter was vertically flipped (replace signal value $s(t)$ by $\max_t\{s(t)\} - s(t)$ for each time point t).

https://doi.org/10.1371/journal.pcbi.1011646.g005

In a typical scenario, we observed an alternation between a single auxin peak and none. Interestingly, there have been observations of controlled cell proliferation in roots, which may increase the synchrony of cell divisions in specific tissues [61]. Similarly, the recently proposed mechanism of "reflux-and-growth" [45, 46] shows how computational simulations on realistic tissue geometries can produce an oscillatory zone under the control of tissue growth.

However, in our simulations, the level of synchrony required to induce robust oscillations proved to be typically much higher than the experimental figures we have found in the literature. By running simulations with plausible variations in cell division sizes (and hence timings), we found again that snake jumping occurs and can lead to alternations between qualitatively distinct auxin maxima. However, the number of distinct snaking diagrams now becomes driven by a stochastic process that leads to an infinite number of configurations, albeit qualitatively similar. This additional complexity makes it impossible to decipher any regular pattern in auxin fluctuations. Yet, fluctuations of significant amplitude did typically occur.

Though these results rely on a fixed set of parameter values and a limited of tissue configurations, an extensive preliminary exploration demonstrates its robustness. From a mathematical point of view, it would be valuable to perform a more systematic analysis, sampling ensembles of parameter choices and initial conditions to confirm the extent to which the behaviours we have observed are parameter-independent. However, the underlying geometric interpretation of the snake jumping effect is largely qualitative and should therefore persist

beyond our current parameter choices, and in fact for entirely different models as well provided they present fold bifurcations whose location depend on the underlying tissue geometry.

This prompted us to produce some experimental validation, which we obtained by means of the DII:Venus reporter. In our experimental time courses, we did indeed observe the same type of irregular auxin fluctuations. We were able to find some surprisingly good qualitative agreement between simulations and experiment. As with any modelling approach, it is inherently impossible to confirm that our modelling proposal is 'true', and there may always be some artifacts due to experimental constraints. But we can state an excellent consistency between the model predictions and the data. This is largely made possible by the qualitative nature of our predictions, which stems from the use of bifurcation methods.

From the present work and others, it appears that the combination of active transport and cell division can lead to a wide range of auxin signals at the single cell level; typically one expects individual cells to perceive neither a steady level of auxin, nor a very regular oscillatory signal. This stands both for modelling and experimental observations. Since ultimately the role of auxin in plants is to trigger responses in individual cells, this general observation naturally leads to the question of how would such complex signals be transduced by the auxin pathway. This is especially intriguing when considering the fact that this pathway is able to oscillate spontaneously with constant auxin inputs, at least in theory: a Hopf bifurcation was found in [58] to give rise to stable oscillations in a differential equation model. In fact, it has been suggested that the DR5 oscillations occur downstream of auxin itself: in [44] the authors include oscillations as an input to an ODE model rather than having them emerge spontaneously, and provide numerical evidence that periodic auxin waves can enhance these oscillations, if they are in phase. The mechanism uncovered here shows how periodic auxin fluctuations can result from the patterns of growth of the tissue.

This opens up the possibility for a complex interplay between rhythms of auxin itself and the protein network it controls. Ultimately, fluctuations of auxin are dependent on the synchronisation between cells undergoing division. In other words, it is the timing of cell mitotic cycles and the spatial distribution of their phase that determine fluctuations of auxin. As a first attempt at exploring growth/divisions in a systematic manner, the present work focuses on simple scenarios, without local differences between cell sizes and division frequencies. This is a necessary simplification from the true complexity of observed in plants. In particular, both the capacity of a cell to elongate and divide depend on its position within the root meristem. It was not possible to include this high degree of complexity within the existing template, but it would be a natural follow-up to consider models with more complex spatial organization, as well as to run experiments involving local disruption of growth.

The respective roles of auxin transport and signalling have been previously acknowledged as potential drivers for auxin patterning and, in particular, oscillations. The present work highlights the importance of patterns of cell division in plant tissues as a third key player underlying auxin distribution dynamics and the many processes it regulates.

Materials and methods

Auxin transport model

The following sections provide equations and formal details about the model used throughout the paper. In addition, a visual schematic is shown in Fig 6.

Main differential equations.   As mentioned earlier, though the notations are slightly adapted, the model presented in this section is based on previous research first published in [38], in particular relying on the bifurcation study performed for this model in [33].
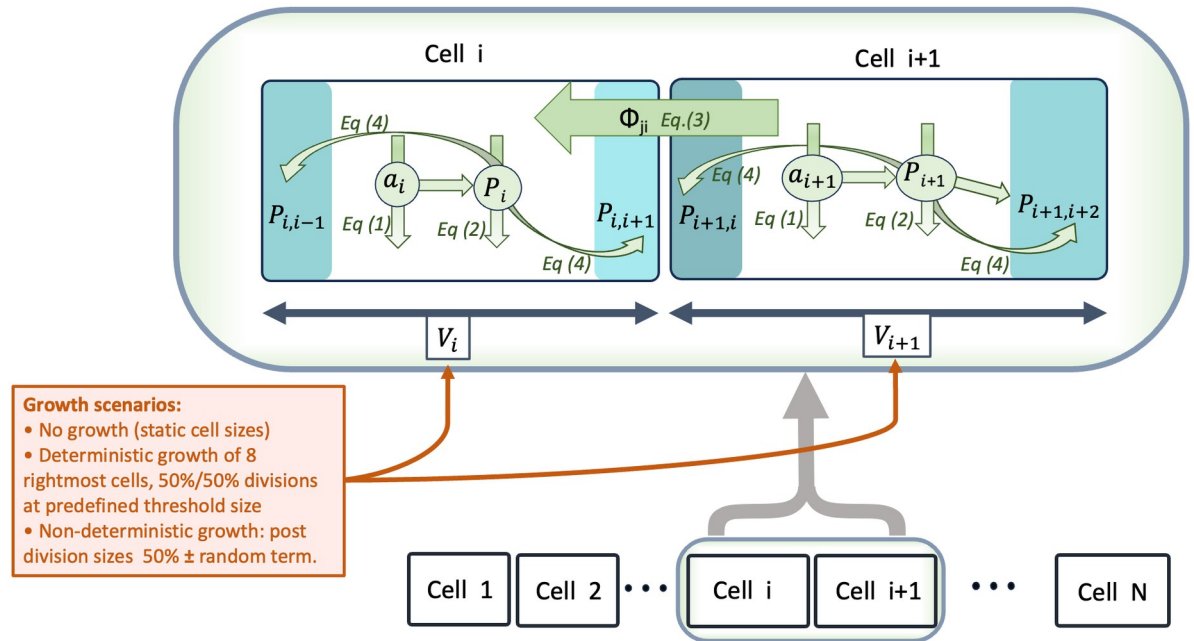
Fig 6. Diagram of the modelled processes. Rectangular boxes represent cells. A zoom on two cells indicates all model variables. Numbered equations from the main text are referenced near the arrows that depict the associated processes, which rule the time evolution of variables. The different growth/division scenarios are also succinctly described, see main text for details.

We consider the active transport of auxin in a tissue composed of $N = N(t)$ cells at time t. Each cell $i \in \mathcal{N}(t) \doteq \{1 \dots N(t)\}$ has neighbours $\mathcal{N}_i = \mathcal{N}_i(t) \subset \mathcal{N}(t)$, therefore inducing a graph $G = G(t)$ with node set $\mathcal{N}(t)$ and edges (i, j) whenever cells i and j are in physical contact, i.e. $i \in \mathcal{N}_j$ or equivalently $j \in \mathcal{N}_i$. We denote by $V_i(t)$ the volume of cell i, and $A_{ij}(t)$ the exchange surface area between cell i and j. Please note that whenever it is not the main point of the discussion, we shall drop the dependence on time to simplify notations.

To describe the dynamics of auxin transport, we use a_i to denote the concentration of auxin and p_i to denote the concentration of transporter proteins (PIN), in a cell i. Thus, any variation of auxin a_i in cell i is due to the interplay between four processes:

- auxin synthesis, whose metabolism is simplified into a Michaelis-Menten rate with saturation constant ρ_{IAA} and Michaelis (i.e. half-maximum) constant κ_{IAA}.

- auxin degradation, with a fixed rate μ_{IAA},

- free diffusion towards neighbouring cells $j \in \mathcal{N}_i$, described using Fick's law: $D(a_i - a_j)$, where D is a permeability coefficient, indicative of diffusion between neighbouring cells,

- active transport by the transporter (PIN) proteins $T(P_{ij}h(a_i, a_j) - P_{ji}h(a_j, a_i))$, where T is a transport efficiency coefficient, P_{ij} is the concentration of PINs in cell i near the interface with cell j and $h(x, y)$ a function taking different forms in the literature (cf. e.g. [26, 27]), see below for the version from [38].

For each cell $i \in \{1, \ldots, N\}$ in the fixed geometry model

$$\frac{da_i}{dt} = \frac{1}{V_i} \sum_{j \in \mathcal{N}_i} \Phi_{ji} + \frac{\rho_{\text{IAA}}}{1 + \kappa_{\text{IAA}} a_i} - \mu_{\text{IAA}} a_i \tag{1}$$

$$\frac{dp_i}{dt} = \frac{\rho_{\text{PIN0}} + \rho_{\text{PIN}} a_i}{1 + \kappa_{\text{PIN}} p_i} - \mu_{\text{PIN}} p_i \tag{2}$$

where Φ_{ij} denotes the flux of auxin from cell i to cell j:

$$\Phi_{ij} = \left(TP_{ij} \frac{a_i}{1 + \kappa_T a_j^2} + DA_{ji} \right) a_i - \left(TP_{ji} \frac{a_j}{1 + \kappa_T a_i^2} + DA_{ji} \right) a_j. \tag{3}$$

and

$$P_{ij} = p_i \frac{A_{ij} \exp(c_1 a_j)}{\sum_{k \in \mathcal{N}_i} A_{ik} \exp(c_1 a_k)}. \tag{4}$$

Throughout the paper, the domain consists of a single file of cells with homogeneous contact surface (normalized to 1), and the following neighbouring structure

$$\mathcal{N}_i = \begin{cases} \{1, 2\} & \text{if} \quad i = 1 \\ \{i-1, i+1\} & \text{if} \quad 2 \leqslant i \leqslant N - 1 \\ \{N-1\} & \text{if} \quad i = N. \end{cases}$$

This choice ensures that cell 1, being its own neighbour, mimics the shootwards end of a root as an open-ended interface, where $\Phi_{11} = 0$ from (3), but with a PIN polarity consistent with there being further cells to the left. On the other hand, the only neighbour of N is $N - 1$ and there is neither flux nor PINs to the right, as would be expected at the root tip.

Implementing growth. Whilst understanding how patterning occurs on a fixed domain is important, many realistic dynamical systems occur on growing domains. In biological tissues, growth typically comprises cell elongation and cell division. Specifically in plant tissues, these can occur over timescales comparable to auxin temporal variations. Indeed in plant roots cell divisions occur with a typical period of 10–53h hours in Arabidopsis [12, 51]. Periodic oscillations of auxin response are also observed to have a period of a few hours, e.g. 15 hours [10] or 6 hours [11], and are critical to the formation of lateral roots. Hence, considering a growing tissue is relevant not only for mathematical purposes, but is also required by the underlying biology. Furthermore, given the nature of auxin transport, with anisotropic, auxin-dependent membrane-bound transporters, continuum approximations are mathematically challenging and seldom attempted, one notable main exception being the 4th order equation derived in [62], which is similar to descriptions of curved elastic shells. Since models including cells as discrete units are by far the most common in the literature, we focus on this approach which also allows to represent cell divisions explicitly.

Regardless of the exact growth model, we must alter the ODEs to take into account dilution due to volume change. Note that concentration is quantity over volume, therefore $a_i = \frac{\hat{a}_i}{V_i}$,

where $\hat{a}_i$ is the quantity of auxin in cell i. Differentiating a_i with respect to time, t gives us:

$$
\begin{aligned}
\frac{da_i}{dt} &= \frac{d}{dt}\frac{\hat{a}_i}{V_i} \\
&= \frac{1}{V_i}\frac{d\hat{a}_i}{dt} - \frac{dV_i}{dt}\frac{\hat{a}_i}{V_i^2} \\
&= \frac{1}{V_i}\frac{d\hat{a}_i}{dt} - \frac{dV_i}{dt}\frac{a_i}{V_i}
\end{aligned}
$$

Therefore, a term $-\frac{dV_i}{dt}\frac{a_i}{V_i}$ must be added to the right-hand side of Eq (1). Similarly, $-\frac{dV_i}{dt}\frac{p_i}{V_i}$ must be introduced in (2).

To mimic growth patterns in roots, one restricts growth to a sub-domain near the tip of the tissue [51]. Note that for theoretical purposes, growth over the whole domain has been considered in [63] and, though not reported in detail here, leads to similar mathematical conclusions as shown here.

We denote the set of dividing cells by $\mathcal{D}(t) \subset \mathcal{N}(t)$, and more precisely $\mathcal{D}(t) = \{N(t) - N_{div}\ldots N(t)\}$, for a fixed N_{div} representing the size of the growing zone. To retain simplicity we considered growth to take place linearly over time, i.e. at a constant rate denoted by g. As in previous simulation studies [38, 41], cells divide when their volume reaches a threshold, here denoted V_{max}. This is in reasonable agreement with experimental data [13]. Thus, the resulting extension of Eqs (1) and (2) with growth and divisions is:

$$
\frac{da_i}{dt} = \frac{1}{V_i}\sum_{j=1}^{N}\Phi_{ji} + \frac{\rho_{\text{IAA}}}{1 + \kappa_{\text{IAA}}a_i} - \mu_{\text{IAA}}a_i - \frac{dV_i}{dt}\frac{a_i}{V_i} \tag{5}
$$

$$
\frac{dp_i}{dt} = \frac{\rho_{\text{PIN0}} + \rho_{\text{PIN}}a_i}{1 + \kappa_{\text{PIN}}p_i} - \mu_{\text{PIN}}p_i - \frac{dV_i}{dt}\frac{p_i}{V_i} \tag{6}
$$

$$
\frac{dV_i}{dt} = \begin{cases} g & \text{if } V_i < V_{max} \text{ and } i \in \mathcal{D}(t), \\ 0 & \text{otherwise,} \end{cases} \tag{7}
$$

with (3) and (4) still used for the fluxes Φ_{ij}. Note that the actual cell subscripts, and those of their neighbours, have to be updated after each division event. Therefore, we would need to specify an algorithm for an arbitrary tissue here. For a linear chain of cells, it is natural that, at any time, cell i is the left neighbour of cell $i + 1$. When a cell divides, its two "daughter cells" are by default initialised with a volume $\frac{V_{max}}{2}$, where auxin and PIN concentrations are equal to that of the parent cell and all cells to the right of a division have their subscript increased by one.

Throughout the paper, the parameter values from Table 1 are used, unless specified.

In practice, for simulations as shown on Figs 2C and 2D or 3A and 3B, the initial condition was 2 cells of volume 1 with auxin and pin concentrations of 1. The time stepping was performed using ode23s (from Matlab) with a step size of 1. Due to the timescale used, as can be seen in the related animations, the system tends relatively fast towards the stable attractors reducing the importance of the initial condition. However, for more complex initial geometries, especially those with high (> 20) numbers of cells, we observed a more significant impact of the initial distribution of auxin, which is explained by the higher number of available steady state branches.

Implementing noise on cell divisions. As real life cell divisions are not expected to occur synchronously, we also implemented a stochastic variant of the previous section, where instead of being $\frac{V_{max}}{2}$ the size of the daughter cells were normally distributed between 24% and 76% of their mother's size. More specifically, the percentage for one of the daughter cells was set to 50+x% where x follows a centred normal distribution with variance σ^2, truncated to enforce $|x| < 26$ (using the `truncate` routine in Matlab). We considered different values for σ, with the highest being derived from a study of cell division in the shoot apical meristem [54] in which a histogram of the proportion daughter cells were of their parents size was a bell curve with a reported standard deviation of $\sigma = 9.3$. Zones of synchronized cell divisions have been reported in the literature [12]. This would suggest a model where the variance σ is not the same throughout the domain. In absence of any quantitative estimates of the spatial distribution of σ, we chose to set it as a single constant.

DII: Venus confocal imaging

We acquired 18 hourly observations, for nine roots of *Arabidopsis thaliana* grown in identical conditions, see [64] for more experimental background.

Plant growth and preparation. DII:Venus seeds cloned using the DEAL vector were sown on 0.5x Murishage and Skoog basal salts with 1% MES monohydrate, 1% agar, pH 5.7. Seeds were then stratified at 4˚C in darkness for 2 days before being placed in a growth chamber at 21˚C with a 16h light, 8h dark regime. 3–4 days after germination and 12 hours prior to imaging, seedlings were transferred to glass-bottomed imaging cuvettes and the root covered with a slice of growth medium gel. They were then returned to their growth conditions overnight.

Imaging and image analysis. Being kept in growth chambers in between imaging sessions, each seedling was imaged once per hour for 18 hours using a Leica SP8 laser scanning confocal microscope with a 40x dry objective. Plants were grown vertically but seedlings were reoriented to horizontal for the time necessary to image (under a minute). Excitation of both VENUS and tdTomato was performed using a 514 nm laser, and emission collected with photomultiplier tube or hybrid detectors across 520–550 nm and 570–760 nm, respectively. Measurements of fluorescence intensity were made using FIJI software to isolate individual nuclei and output mean gray values.

Three of the authors then recorded manually, for each root, three groups of five cells from the cortex, from the tip upwards, for each time point. This was performed using standard selection and measurement tools in Fiji [65]. We aggregated the three data sets to account for variations between the three records, which were unavoidable due to the experimental noise present in some images, making the boundary of a cell or nucleus partly blurry. In addition, we quantified DII intensity in cells from the stele. This was done by selecting the whole stele that was visible between the QC and the 5th cortex cell.

Raw images: Confocal images are available using the following permanent link: https://doi.org/10.17632/p7ftp5wm3h.1.

Supporting information

S1 Fig. Bifurcation diagram: Unstable branches. A refined and zoomed version of Fig 1 showing additional, unstable branches.
(JPG)

S2 Fig. Additional bifurcation diagrams. As a complement to Fig 2, alternative diagrams are included. (A) Continuation in T for a domain comprising 16 groups of 8 identical cells whose

volume increase from 1 (8 tip cells) to 10 (leftmost 8 cells). (B) Steady state (auxin concentration) for $T \approx 20$; the larger cells require higher transport rates to create multiple auxin maxima. Patterns for lower T have fewer auxin peaks. Cell sizes are represented in the insert. (C) Continuation using cell volume as control parameter can be used to illustrate the creation/annihilation of auxin peaks leading to an oscillatory signal. Axes labels are self-explanatory, $T = 2$.
(PNG)

S3 Fig. Full time series for Fig 5. As a heatmap; same legend as Figs 2 and 3. The plots from Fig 5 were obtained by extracting intervals of 200 time units (min) from this time series with random cell division (with $\sigma = 9.3$). The graphs were generated by randomly picking start points throughout the simulation such that they would not overlap with any other interval and plotting the mean auxin over cells 6–10, for the selected 200min interval.
(TIF)

S1 File. Dynamical systems glossary. Some background on dynamical systems theory, presented for non-mathematicians.
(PDF)

S2 File. Matlab code. The code used for all time-stepping and continuation methods. Note that the latter requires some more specialised techniques than available by default in e.g. Matlab. We relied on a previously published implementation by one of the authors (DA); see the publicly available Matlab files from [49], which come with a complete set of tutorials and technical references.
(ZIP)

S3 File. Processed imaging data. The measured fluorescence data as an excel file. **Sheet 1**: The first three columns indicate the root, domain (out of three groups of 5 cells) and time point recorded. The following columns record the mean DII intensity, its standard deviation (within the domain) and the surface area of the selected domain, with three repeats for the three authors replicating the analysis. Final columns compute a pooled standard deviation from the three repeats, using the pixel size from confocal images to estimate number of measured pixels from the surface area. **'Stele' sheet**: contains a single measurement of the DII intensity in the stele area, for each root and time point.
(XLSX)

S1 Video. Stable patterns along the snaking diagram. The stable patterns of auxin, including those in Fig 1A, are displayed as the animation follows the steps of the continuation algorithm underlying the making of Fig 1B.
(MP4)

S2 Video. Auxin oscillations induced by cell divisions. Animation representing the simulated growing root with synchronized cell divisions from Fig 2B–2D; all three values of T are superimposed, with legend within the animation.
(MP4)

S3 Video. Deformations of snaking under tissue growth: Deterministic case. Animation representing the deformations of the snaking diagram as the domain grows. The crosses follows the time course simulations from Fig 2B–2D, with corresponding T values in legend.
(MP4)

S4 Video. Deformations of snaking under tissue growth: Low σ. Animation representing the deformations of the snaking diagram as the domain grows as in Fig 3A; $T = 1.9$, $\sigma = 2.325$. The red cross follows the time course simulation, which departs transiently from equilibrium

branches when they are rapidly updated.
(MP4)

S5 Video. Deformations of snaking under tissue growth: Physiological σ. Animation representing the deformations of the snaking diagram as the domain grows as in Fig 3B; T = 1.9, $σ$ = 9.3. The red cross follows the time course simulation, which departs transiently from equilibrium branches when they are rapidly updated.
(MP4)

Author Contributions

Conceptualization: Simon Bellows, Daniele Avitabile, John R. King, Anthony Bishopp, Etienne Farcot.

Formal analysis: Simon Bellows, Daniele Avitabile, John R. King, Anthony Bishopp, Etienne Farcot.

Funding acquisition: John R. King, Anthony Bishopp, Etienne Farcot.

Investigation: Simon Bellows, George Janes, Anthony Bishopp.

Methodology: Simon Bellows, Daniele Avitabile, John R. King, Anthony Bishopp, Etienne Farcot.

Project administration: Etienne Farcot.

Software: Simon Bellows, Daniele Avitabile.

Supervision: Daniele Avitabile, John R. King, Anthony Bishopp, Etienne Farcot.

Validation: George Janes.

Writing – original draft: Simon Bellows, Anthony Bishopp, Etienne Farcot.

Writing – review & editing: George Janes, John R. King, Anthony Bishopp, Etienne Farcot.

References

1. Abel S, Theologis A. Odyssey of auxin. Cold Spring Harbor Perspectives in Biology. 2010; 2(10): a004572. https://doi.org/10.1101/cshperspect.a004572 PMID: 20739413

2. Dupré J. Processes of life: Essays in the philosophy of biology. Oxford University Press; 2012.

3. Jaeger J, Monk N. Everything flows: A process perspective on life. EMBO reports. 2015; 16(9):1064–1067. https://doi.org/10.15252/embr.201541088 PMID: 26276845

4. Letellier C, Abraham R, Shepelyansky DL, Rössler OE, Holmes P, Lozi R, et al. Some elements for a history of the dynamical systems theory. Chaos: An Interdisciplinary Journal of Nonlinear Science. 2021; 31(5):053110. https://doi.org/10.1063/5.0047851 PMID: 34240941

5. Casanova-Sáez R, Mateo-Bonmatí E, Ljung K. Auxin metabolism in plants. Cold Spring Harbor Perspectives in Biology. 2021; 13(3):a039867. https://doi.org/10.1101/cshperspect.a039867 PMID: 33431579

6. Leyser O. Auxin signaling. Plant physiology. 2018; 176(1):465–479. https://doi.org/10.1104/pp.17.00765 PMID: 28818861

7. Kubeš M, Napier R. Non-canonical auxin signalling: fast and curious. Journal of Experimental Botany. 2019; 70(10):2609. https://doi.org/10.1093/jxb/erz111 PMID: 30854547

8. Friml J. Auxin transport—shaping the plant. Current opinion in plant biology. 2003; 6(1):7–12. https://doi.org/10.1016/S1369526602000031 PMID: 12495745

9. Abel S, Nguyen MD, Theologis A. The PS-IAA4/5-like Family of Early Auxin-inducible mRNAs in Arabidopsis thaliana. Journal of molecular biology. 1995; 251(4):533–549. https://doi.org/10.1006/jmbi.1995.0454 PMID: 7658471

10. De Smet I, Tetsumura T, De Rybel B, dit Frey N, Laplaze L, Casimiro I, et al. Auxin-dependent regulation of lateral root positioning in the basal meristem of Arabidopsis. Development. 2007; 134(4):681–690. https://doi.org/10.1242/dev.02753 PMID: 17215297

11. Moreno-Risueno MA, Van Norman JM, Moreno A, Zhang J, Ahnert SE, Benfey PN. Oscillating gene expression determines competence for periodic Arabidopsis root branching. Science. 2010; 329 (5997). https://doi.org/10.1126/science.1191937 PMID: 20829477

12. Rahni R, Birnbaum KD. Week-long imaging of cell divisions in the Arabidopsis root meristem. Plant Methods. 2019; 15:1–14. https://doi.org/10.1186/s13007-019-0417-9 PMID: 30988691

13. Pavelescu I, Vilarrasa-Blasi J, Planas-Riverola A, González-García MP, Caño-Delgado AI, Ibañes M. A Sizer model for cell differentiation in Arabidopsis thaliana root growth. Molecular systems biology. 2018; 14(1):e7687. https://doi.org/10.15252/msb.20177687 PMID: 29321184

14. Kramer EM, Rutschow HL, Mabie SS. AuxV: a database of auxin transport velocities. Trends in plant science. 2011; 16(9):461–463. https://doi.org/10.1016/j.tplants.2011.05.003 PMID: 21684188

15. Turing A. The Chemical Basis of Morphogenesis. Philosophical Transactions of the Royal Society of London Series B. 1952; 237(641):37–72. https://doi.org/10.1098/rstb.1952.0012

16. Crampin EJ, Gaffney EA, Maini PK. Reaction and diffusion on growing domains: scenarios for robust pattern formation. Bulletin of mathematical biology. 1999; 61(6):1093–1120. https://doi.org/10.1006/bulm.1999.0131 PMID: 17879872

17. Crampin E, Hackborn W, Maini P. Pattern formation in reaction-diffusion models with nonuniform domain growth. Bulletin of mathematical biology. 2002; 64(4):747–769. https://doi.org/10.1006/bulm.2002.0295 PMID: 12216419

18. Madzvamuse A, Gaffney EA, Maini PK. Stability analysis of non-autonomous reaction-diffusion systems: the effects of growing domains. Journal of mathematical biology. 2010; 61(1):133–164. https://doi.org/10.1007/s00285-009-0293-4 PMID: 19727733

19. Plaza RG, Sanchez-Garduno F, Padilla P, Barrio RA, Maini PK. The effect of growth and curvature on pattern formation. Journal of Dynamics and Differential Equations. 2004; 16(4):1093–1121. https://doi.org/10.1007/s10884-004-7834-8

20. Ueda KI, Nishiura Y. A mathematical mechanism for instabilities in stripe formation on growing domains. Physica D: Nonlinear Phenomena. 2011; 241(1). https://doi.org/10.1016/j.physd.2011.09.016

21. Krause AL, Gaffney EA, Maini PK, Klika V. Introduction to 'Recent progress and open frontiers in Turing's theory of morphogenesis'. Philosophical Transactions of the Royal Society A. 2021; 379 (2213):20200280. https://doi.org/10.1098/rsta.2020.0280 PMID: 34743606

22. Seirin Lee S, Gaffney EA, Baker RE. The dynamics of Turing patterns for morphogen-regulated growing domains with cellular response delays. Bulletin of mathematical biology. 2011; 73:2527–2551. https://doi.org/10.1007/s11538-011-9634-8 PMID: 21347815

23. Van Gorder RA, Klika V, Krause AL. Turing conditions for pattern forming systems on evolving manifolds. Journal of mathematical biology. 2021; 82:1–61. https://doi.org/10.1007/s00285-021-01552-y PMID: 33475826

24. Krause AL, Ellis MA, Van Gorder RA. Influence of curvature, growth, and anisotropy on the evolution of Turing patterns on growing manifolds. Bulletin of mathematical biology. 2019; 81:759–799. https://doi.org/10.1007/s11538-018-0535-y PMID: 30511207

25. Krause AL, Gaffney EA, Walker BJ. Concentration-Dependent Domain Evolution in Reaction–Diffusion Systems. Bulletin of Mathematical Biology. 2023; 85(2):14. https://doi.org/10.1007/s11538-022-01115-2 PMID: 36637542

26. van Berkel K, de Boer RJ, Scheres B, ten Tusscher K. Polar auxin transport: models and mechanisms. Development. 2013; 140(11):2253–2268. https://doi.org/10.1242/dev.079111 PMID: 23674599

27. Mitchison G. The polar transport of auxin and vein patterns in plants. Phil Trans R Soc Lond B. 1981; 295(1078):461–471. https://doi.org/10.1098/rstb.1981.0154

28. Heisler MG, Jönsson H. Modeling auxin transport and plant development. Journal of Plant Growth Regulation. 2006; 25(4):302–312.

29. Sahlin P, Söderberg B, Jönsson H. Regulated transport as a mechanism for pattern generation: capabilities for phyllotaxis and beyond. Journal of theoretical biology. 2009; 258(1):60–70. https://doi.org/10.1016/j.jtbi.2009.01.019 PMID: 19490869

30. Walker ML, Farcot E, Traas J, Godin C. The flux-based PIN allocation mechanism can generate either canalyzed or diffuse distribution patterns depending on geometry and boundary conditions. PloS one. 2013; 8(1):e54802. https://doi.org/10.1371/journal.pone.0054802 PMID: 23382973

31. Feller C, Gabriel JP, Mazza C, Yerly F. Pattern formation in auxin flux. Journal of mathematical biology. 2014; 68(4):879–909. https://doi.org/10.1007/s00285-013-0655-9 PMID: 23436057

32. Farcot E, Yuan Y. Homogeneous auxin steady states and spontaneous oscillations in flux-based auxin transport models. SIAM Journal on Applied Dynamical Systems. 2013; 12(3):1330–1353. https://doi.org/10.1137/120891538

33. Draelants D, Avitabile D, Vanroose W. Localized auxin peaks in concentration-based transport models of the shoot apical meristem. Journal of the Royal Society, Interface. 2015; 12(106). https://doi.org/10.1098/rsif.2014.1407 PMID: 25878130

34. Galvan-Ampudia CS, Cerutti G, Legrand J, Brunoud G, Martin-Arevalillo R, Azais R, et al. Temporal integration of auxin information for the regulation of patterning. Elife. 2020; 9:e55832. https://doi.org/10.7554/eLife.55832 PMID: 32379043

35. Bhatia N, Heisler MG. Self-organizing periodicity in development: organ positioning in plants. Development. 2018; 145(3):dev149336. https://doi.org/10.1242/dev.149336 PMID: 29439134

36. Bakker BH, Faver TE, Hupkes HJ, Merks RM, van der Voort J. Scaling relations for auxin waves. Journal of Mathematical Biology. 2022; 85(4):1–72. https://doi.org/10.1007/s00285-022-01793-5 PMID: 36163567

37. Allen HR, Ptashnyk M. Mathematical Modelling of Auxin Transport in Plant Tissues: Flux Meets Signalling and Growth. Bulletin of Mathematical Biology. 2020; 82(2):17. https://doi.org/10.1007/s11538-019-00685-y PMID: 31970524

38. Smith RS, Guyomarc'h S, Mandel T, Reinhardt D, Kuhlemeier C, Prusinkiewicz P. A plausible model of phyllotaxis. Proceedings of the National Academy of Sciences. 2006; 103(5):1301–1306. https://doi.org/10.1073/pnas.0510457103 PMID: 16432192

39. Jönsson H, Heisler MG, Shapiro BE, Meyerowitz EM, Mjolsness E. An auxin-driven polarized transport model for phyllotaxis. Proceedings of the National Academy of Sciences. 2006; 103(5):1633–1638. https://doi.org/10.1073/pnas.0509839103 PMID: 16415160

40. Barbier de Reuille P, Bohn-Courseau I, Ljung K, Morin H, Carraro N, Godin C, et al. Computer simulations reveal properties of the cell-cell signaling network at the shoot apex in Arabidopsis. Proceedings of the National Academy of Sciences. 2006; 103(5):1627–1632. https://doi.org/10.1073/pnas.0510130103

41. Stoma S, Lucas M, Chopard J, Schaedel M, Traas J, Godin C. Flux-Based Transport Enhancement as a Plausible Unifying Mechanism for Auxin Transport in Meristem Development (Flux-Based Polarization in Meristem Development). PLoS Computational Biology. 2008; 4(10). https://doi.org/10.1371/journal.pcbi.1000207 PMID: 18974825

42. Band LR, King JR. Multiscale modelling of auxin transport in the plant-root elongation zone. Journal of mathematical biology. 2012; 65(4):743–785. https://doi.org/10.1007/s00285-011-0472-y PMID: 22015980

43. Twycross J, Band LR, Bennett MJ, King JR, Krasnogor N. Stochastic and deterministic multiscale models for systems biology: an auxin-transport case study. BMC Systems Biology. 2010; 4(1):1–11. https://doi.org/10.1186/1752-0509-4-34 PMID: 20346112

44. Perianez-Rodriguez J, Rodriguez M, Marconi M, Bustillo-Avendaño E, Wachsman G, Sanchez-Corrionero A, et al. An auxin-regulable oscillatory circuit drives the root clock in Arabidopsis. Science Advances. 2021; 7(1):eabd4722. https://doi.org/10.1126/sciadv.abd4722 PMID: 33523850

45. van den Berg T, Yalamanchili K, de Gernier H, Santos Teixeira J, Beeckman T, Scheres B, et al. A reflux-and-growth mechanism explains oscillatory patterning of lateral root branching sites. Developmental cell. 2021; 56(15):2176–2191.e10. https://doi.org/10.1016/j.devcel.2021.07.005 PMID: 34343477

46. Santos Teixeira J, van den Berg T, Ten Tusscher K. Complementary roles for auxin and auxin signalling revealed by reverse engineering lateral root stable prebranch site formation. Development. 2022; 149(22):dev200927. https://doi.org/10.1242/dev.200927 PMID: 36314783

47. Brunoud G, Wells DM, Oliva M, Larrieu A, Mirabet V, Burrow AH, et al. A novel sensor to map auxin response and distribution at high spatio-temporal resolution. Nature. 2012; 482(7383):103–106. https://doi.org/10.1038/nature10791 PMID: 22246322

48. Rankin J, Avitabile D, Baladron J, Faye G, Lloyd DJ. Continuation of localized coherent structures in nonlocal neural field equations. SIAM Journal on Scientific Computing. 2014; 36(1):B70–B93. https://doi.org/10.1137/130918721

49. Avitabile D. Numerical Computation of Coherent Structures in Spatially-Extended Systems (v1.0). doi.org/10.5281/zenodo.3821164. Zenodo. 2020.

50. Houghton SM, Knobloch E. Homoclinic snaking in bounded domains. Physical review E, Statistical, nonlinear, and soft matter physics. 2009; 80(2 Pt 2):026210. https://doi.org/10.1103/PhysRevE.80.026210 PMID: 19792234

51. Beemster GT, Baskin TI. Analysis of cell division and elongation underlying the developmental acceleration of root growth in Arabidopsis thaliana. Plant physiology. 1998; 116(4). https://doi.org/10.1104/pp.116.4.1515 PMID: 9536070

52. Avitabile D, Lloyd DJ, Burke J, Knobloch E, Sandstede B. To snake or not to snake in the planar Swift–Hohenberg equation. SIAM Journal on Applied Dynamical Systems. 2010; 9(3):704–733. https://doi.org/10.1137/100782747

53. Socha JJ. Gliding flight in Chrysopelea: turning a snake into a wing. Integrative and Comparative Biology. 2011; 51(6):969–982. https://doi.org/10.1093/icb/icr092 PMID: 21816808

54. Shapiro BE, Tobin C, Mjolsness E, Meyerowitz EM. Analysis of cell division patterns in the Arabidopsis shoot apical meristem. Proceedings of the National Academy of Sciences. 2015; 112(15). https://doi.org/10.1073/pnas.1502588112 PMID: 25825722

55. von Wangenheim D, Hauschild R, Fendrych M, Barone V, Benková E, Friml J. Live tracking of moving samples in confocal microscopy for vertically grown roots. eLife. 2017; 6:e26792. https://doi.org/10.7554/eLife.26792 PMID: 28628006

56. Campilho A, Garcia B, Toorn HVD, Wijk HV, Campilho A, Scheres B. Time-lapse analysis of stem-cell divisions in the Arabidopsis thaliana root meristem. The Plant journal: for cell and molecular biology. 2006; 48(4). https://doi.org/10.1111/j.1365-313X.2006.02892.x PMID: 17087761

57. Liao CY, Smet W, Brunoud G, Yoshida S, Vernoux T, Weijers D. Reporters for sensitive and quantitative measurement of auxin response. Nature methods. 2015; 12(3):207–210. https://doi.org/10.1038/nmeth.3279 PMID: 25643149

58. Middleton AM, King JR, Bennett MJ, Owen MR. Mathematical modelling of the Aux/IAA negative feedback loop. Bulletin of mathematical biology. 2010; 72(6):1383–1407. https://doi.org/10.1007/s11538-009-9497-4 PMID: 20135237

59. Farcot E, Lavedrine C, Vernoux T. A modular analysis of the auxin signalling network. PLoS One. 2015; 10(3):e0122231. https://doi.org/10.1371/journal.pone.0122231 PMID: 25807071

60. Band LR, Wells DM, Larrieu A, Sun J, Middleton AM, French AP, et al. Root gravitropism is regulated by a transient lateral auxin gradient controlled by a tipping-point mechanism. Proceedings of the National Academy of Sciences. 2012; 109(12):4668–4673. https://doi.org/10.1073/pnas.1201498109 PMID: 22393022

61. Xuan W, Band LR, Kumpf RP, Van Damme D, Parizot B, De Rop G, et al. Cyclic programmed cell death stimulates hormone signaling and root development in Arabidopsis. Science. 2016; 351(6271):384–387. https://doi.org/10.1126/science.aad2776 PMID: 26798015

62. Newell AC, Shipman PD, Sun Z. Phyllotaxis: cooperation and competition between mechanical and biochemical processes. Journal of theoretical biology. 2008; 251(3):421–439. https://doi.org/10.1016/j.jtbi.2007.11.036 PMID: 18207165

63. Bellows S. Mathematical Modelling of Auxin Signalling and Transport [PhD thesis]. School of Mathematical Sciences. University of Nottingham; 2022.

64. Kümpers BM, Han J, Vaughan-Hirsch J, Redman N, Ware A, Atkinson JA, et al. Dual expression and anatomy lines allow simultaneous visualization of gene expression and anatomy. Plant Physiology. 2022; 188(1):56–69. https://doi.org/10.1093/plphys/kiab503 PMID: 34718789

65. Schindelin J, Arganda-Carreras I, Frise E, Kaynig V, Longair M, Pietzsch T, et al. Fiji: an open-source platform for biological-image analysis. Nature methods. 2012; 9(7):676–682. https://doi.org/10.1038/nmeth.2019 PMID: 22743772